Electronic Supplementary Material (ESI) for Materials Chemistry Frontiers.

Supporting Information

The design of extended Multiple Resonance Thermally Activated Delayed Fluorescence emitter based on polycyclic amine/carbonyl system

Dianming Sun,[a,b] Subeesh Madayanad Suresh,[b] David Hall,[b,c] Ming Zhang,[a] Changfeng Si,[b] David B. Cordes,[b] Alexandra M. Z. Slawin,[b] Yoann Olivier,[c,d*] Xiaohong Zhang[a*] and Eli Zysman-Colman[b*]

[a] *Institute of Functional Nano & Soft Materials (FUNSOM) and Jiangsu Key Laboratory for Carbon-Based Functional Materials & Devices, Soochow University, Suzhou, Jiangsu 215123, P.R. China.* *E-mail: xiaohong_zhang@suda.edu.cn

[b] *Organic Semiconductor Centre, EaStCHEM School of Chemistry, University of St Andrews, St Andrews KY16 9ST, UK.* *E-mail: eli.zysman-colman@st-andrews.ac.uk; http://www.zysman-colman.com

[c] *Laboratory for Chemistry of Novel Materials, University of Mons, 7000, Mons, Belgium*

[d] *Unité de Chimie Physique Théorique et Structurale & Laboratoire de Physique du Solide, Namur Institute of Structured Matter, Université de Namur, Rue de Bruxelles, 61, 5000 Namur, Belgium.*

Table of Contents

General methods **3**

Experimental Section **6**

Theoretical calculation **9**

Photophysical characterization **12**

Reference **26**

General methods

Synthesis and characterization. All commercial chemicals were used as received without further purification. Synthesis of compound **3** and **DDiKTa** were performed using standard Schlenk techniques under nitrogen atmosphere. Dry solvents were collected from solvent purification system. Column chromatography was performed using silica gel (Silia-P from Silicycle, 60 Å, 40 to 63 μm). Analytical thin layer chromatography (TLC) was performed with silica plates on polymer matrix (250 μm with indicator F-254), and compounds were checked under UV light-254 and -365 nm. ^{1}H and ^{13}C solution-phase NMR spectra were recorded on a Bruker Avance spectrometer operating at 11.7 T (Larmor frequencies of 400 MHz and 101MHz or 500 MHz and 126 MHz, respectively) in $CDCl_3$ and CD_2Cl_2. The following abbreviations have been used for multiplicity assignments: "s" for singlet, "d" for doublet, "t" for triplet, "m" for multiplet, and "br" for broad. Melting points (Mps) were recorded using open-ended capillaries on an electrothermal melting point apparatus and are uncorrected.

Electrochemistry measurements. Cyclic Voltammetry (CV) and Differential pulse voltammetry (DPV) analysis were performed on an Electrochemical Analyzer potentiostat model 620D from CH Instruments. The sample was prepared in dichloromethane (DCM) solution, which was degassed by sparging with DCM-saturated nitrogen gas for 5 minutes prior to measurement. All measurements were performed using 0.1 M tetra-*n*-butylammonium hexafluorophosphate, $[n\mathrm{Bu_4N}]PF_6$. An Ag/Ag^+ electrode was used as the reference electrode; a glassy carbon electrode was used as the working electrode and a platinum electrode was used as the counter electrode. The redox potentials are reported relative to a saturated calomel electrode (SCE) with a ferrocene/ferrocenium (Fc/Fc^+) redox couple as the internal standard (0.46 V vs SCE).[1] The HOMO and LUMO energies were determined using the relation $E_{HOMO/LUMO} = -(E_{ox} / E_{red} + 4.8)$ eV, where E_{ox} and E_{red} are the values of the anodic and cathodic peak potentials, respectively calculated from DPV relative to Fc/Fc^+.[2]

Quantum chemical calculations. The calculations were performed with the Gaussian 09 revision D.018 suite[3] for the Density Functional Theory (DFT) calculations and with the Turbomole/6.5 package[3] for Spin-Component Scaling Coupled-Cluster second-order approximate Coupled-Cluster (SCS-CC2) calculations.

Molecular orbitals isocontour plots were obtained based on the gas-phase ground state-optimized structures using the PBE0 functional[4] and the 6-31G (d, p) basis set[5] in the gas phase. Molecular orbitals were visualized using GaussView 5.0.[6] Excited state calculations were performed using the SCS-CC2 method with the cc-pVDZ basis set.[7] We first optimized the ground state at the SCS-CC2 level and vertical transitions to excited states were calculated based on the SCS-CC2 optimized ground state-optimized structure. Difference density plots were used to track the change in electronic density between the ground and the singlet or triplet excited states and were visualized using the VESTA package.[8]

Photophysical measurements. All samples were prepared in HPLC grade solvents with varying concentrations on the order of 10^{-5} or 10^{-6} M for absorption and emission study. Absorption spectra were recorded at RT using a Shimadzu UV-1800 double beam spectrophotometer with a 1 cm quartz cuvette. Molar absorptivity determination was verified by linear least-squares fit of values obtained from at least five independent solutions at varying concentrations on the order of 2.30×10^{-5} to 8.44×10^{-5} M. For emission studies, aerated solutions were bubbled by compressed air for 5 minutes and degassed solutions were prepared via three freeze-pump-thaw cycles and spectra were taken using home-made Schlenk quartz cuvette. Steady-state emission and excitation spectra and time-resolved emission spectra were recorded at 298 K using an Edinburgh Instruments F980 fluorimeter. Samples were excited at 340 nm using a Xenon lamp for steady-state measurements and at 378 nm using a pico-second laser (PicoQuant, LDH-D-C-375) driven by a laser driver (PDL 800-D) for time-resolved emission spectra. The singlet-triplet splitting energy, ΔE_{ST}, was determined from the energy difference between the onsets of the prompt fluorescence and the delayed phosphorescence spectra in toluene glass at 77 K using a Jasco FP-8600 fluorimeter. Photoluminescence quantum yields for solutions were determined using the optically dilute method[9] in which four sample solutions with absorbances of ca. 0.10, 0.080, 0.060 and 0.040 at 340 nm were used. Their emission intensities were compared with those of a reference, quinine sulfate, whose quantum yield (Φ_r) in 1 N H_2SO_4 was determined to be 54.6% using absolute method.[10] The quantum yield of the sample, Φ_{PL}, can be determined by the equation $\Phi_{PL}=\Phi_r(A_r/A_s)(I_s/I_r)(n_s/n_r)^2$, where A stands for the absorbance at the excitation wavelength (λ_{exc}=340 nm), I is the integrated area under the corrected emission curve and n is the refractive index of the solvent with the subscripts “s” and “r” representing sample and reference respectively. Film sample was prepared on sapphire

substrates and cooled to 77 K in a cold finger cryostat (Oxford Instruments). The sample was photoexcited using a femtosecond laser emitting at 343 nm (Orpheus-N, model: PN13F1). Emission from the sample was focused onto a spectrograph (Chromex imaging, 250 is spectrograph) and detected with a sensitive gated iCCD camera (Stanford Computer Optics, 4Picos) having sub-nanosecond resolution. Prompt fluorescence spectra were integrated by the iCDD for 10 ns – 100 ns after the laser excitation. Phosphorescence spectra were integrated by the iCDD for 1 ms – 10 ms after the laser excitation. Thin film Φ_{PL} measurements were performed using an integrating sphere in a Hammamatsu C9920-02 system.[11] Samples were excited at 340 nm by a xenon lamp coupled to a monochromator. The output was then fed into the integrating sphere via a fiber, exciting the sample. The PL was collected with a multimode fiber and detected with a back-thinned CCD (BT-CCD) detector. The thin film Φ_{PL} were then measured by purging the integrating sphere with N_2 gas flow.

X-Ray crystallography. Crystals of Compound **2** were obtained by diffusing hexane into a saturated solution of compound **2** in chloroform. X-ray diffraction data were collected at 173 K using a Rigaku FR-X Ultrahigh brilliance Microfocus RA generator/confocal optics with XtaLAB P200 diffractometer [Mo Kα radiation (λ = 0.71075 Å)]. Intensity data were collected using ω-steps accumulating area detector images spanning at least a hemisphere of reciprocal space. Data were collected using CrystalClear[12] and processed (including correction for Lorentz polarization and absorption) using CrysAlisPro.[13] Structures were solved by dual-space methods (SHELXT-2018/2)[15] and refined by full-matrix least-squares against F^2 (SHELXL-2018/3). Non-hydrogen atoms were refined anisotropically, and hydrogen atoms were refined using a riding model. All calculations were performed using the Olex2[15] interface. A view of the structure is presented in Figure S16. CCDC 1992507 contains the supplementary crystallographic data for this paper. The data can be obtained free of charge from The Cambridge Crystallographic Data Centre via www.ccdc.cam.ac.uk/structures.

Crystal data. $C_{20}H_{10}INO_2$, M = 423.19, triclinic, a = 8.0823(2), b = 8.3105(2), c = 11.8907(4) Å, α = 83.340(2), β = 80.164(2), γ = 69.285(2) °, U = 734.72(4) Å^3, T = 173 K, space group $P\bar{1}$ (no. 2), Z = 2, 9702 reflections measured, 3241 unique (R_{int} = 0.0382), which were used in all calculations. The final R_1 [$I > 2\sigma(I)$] was 0.0326 and wR_2 (all data) was 0.0795.

OLED fabrication and characterization. OLED devices were fabricated in bottom-emitting architecture. A pre-patterned indium tin oxide (ITO) glass substrate with a sheet resistance of 15 Ω square^{-1} was pre-cleaned

carefully with detergent and deionized water and then exposed to UV-ozone for 15 min. The small molecules for each layer were thermally evaporated using a vacuum chamber with a base pressure of 4×10^{-4} Pa and deposited at a rate of 1 Å/s, which was controlled in situ using the quartz crystal monitors. The electron injection layer, LiF, was deposited at a rate of 0.1 Å/s while the Al cathode was deposited at a rate of 10 Å/s through the shadow mask defining the top electrode. The spatial overlap of the anode and cathode electrodes determined the active area of the OLED, which was estimated to be 9 mm^2. Electroluminescence (EL), CIE colour coordinates, and spectra were obtained via a Spectrascan PR655 photometer and the luminance-current-voltage characteristics were determined with a computer-controlled Keithley 2400 Source meter. The external quantum yield (EQE) was calculated from the current density, luminance, and EL spectrum, assuming a Lambertian emission distribution.

Experimental Section

Synthesis of dimethyl 2,2'-((4-iodophenyl)azanediyl)dibenzoate (1)

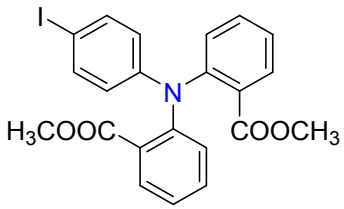

To a 100 mL two-neck flask were added dimethyl 2,2'-(phenylazanediyl)dibenzoate (3.6 g, 10 mmol, 1 equiv.) and 30 mL acetonitrile. After dissolution, *N*-iodosuccinimide (2.7 g, 12 mmol, 1.2 equiv.) dissolved in 20 mL acetonitrile was added dropwise. The reaction was stirred at room temperature for 12 h. The reaction was quenched with 10 mL 0.1 M sodium hydroxide solution and extracted with 50 mL DCM. The organic layer was separated, washed by water (3 × 50 mL), dried with anhydrous magnesium sulfate and concentrated under reduced pressure. The crude product was purified by silica gel column chromatography (hexane: ethyl acetate = 10:1) to afford the desired product as a white solid. **Yield**: 85% (3.1 g). $\mathbf{R_f}$: 0.49 (hexane: ethyl acetate = 5:2). $\mathbf{M_p}$: 130-131 °C. **^{1}H NMR** (500 MHz, CD_2Cl_2) δ 7.71 (dd, *J* = 7.7, 1.7 Hz, 2H), 7.49 (ddd, *J* = 8.1, 7.4, 1.7 Hz, 2H), 7.46 – 7.42 (m, 2H), 7.27 – 7.21 (m, 4H), 6.52 – 6.48 (m, 2H), 3.46 (s, 6H). **^{13}C NMR** (126 MHz, CD_2Cl_2) δ 167.29, 148.56, 145.65, 137.60, 132.81, 130.96, 129.08, 128.20, 124.70, 121.85, 83.12, 53.89, 53.68, 53.46, 53.25, 53.03, 51.75.

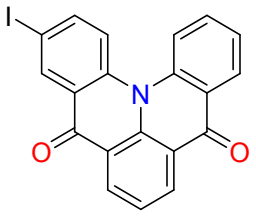

Synthesis of 3-iodoquinolino[3,2,1-de]acridine-5,9-dione (2)

Compound **1** (1.8 g, 5 mmol, 1 equiv.) was combined with sodium hydroxide (1 g, 25 mmol, 5 equiv.) in 20 mL of an ethanol/water (1:1) mixture. The reaction was heated to reflux for 12 h. After cooling to room temperature, the pH was adjusted to 2-3 by addition of dilute hydrochloric acid (HCl). The diacid solid precipitated from the solution and was collected by vacuum filtration, washed thoroughly with water to remove residual salts and HCl and then dried under vacuum. This solid was then used directly by dispersing it into 60 mL dichloromethane under a nitrogen atmosphere. To the reaction mixture were added sequentially thionyl chloride (0.7 mL, 10.0 mmol, 2 equiv.) and a few drops of DMF. After 3 h under reflux, the reaction mixture was cooled to room temperature. Under a positive flow of nitrogen, aluminum chloride (6.7 g, 50 mmol, 10 equiv.) was added slowly (exothermic reaction). The reaction mixture was brought to reflux and stirred for 12 h. The reaction mixture was cooled to room temperature and the reaction was quenched by dropwise addition of water with vigorous

stirring (exothermic reaction). The resulting mixture was extracted with dichloromethane (3 × 50 mL), the organic fraction was separated and then concentrated under reduced pressure. The mixture was then washed with hexane and recrystallized from boiling THF. The crystals were filtered to afford the desired product as a yellow solid. **Yield**: 42% (0.89 g). **R_f**: 0.34 (hexane: ethyl acetate=5:2). **Mp**: 284-285 °C. **^{1}H NMR** (400 MHz, $CDCl_3$) δ 8.93 – 8.84 (m, 3H), 8.56 (dd, *J* = 8.0, 1.6 Hz, 1H), 8.17 (dd, *J* = 8.6, 0.9 Hz, 1H), 8.08 (dd, *J* = 9.0, 2.1 Hz, 1H), 7.99 (d, *J* = 9.0 Hz, 1H), 7.88 – 7.78 (m, 2H), 7.64 (ddd, *J* = 8.0, 7.1, 1.0 Hz, 1H). **^{13}C NMR** (101 MHz, $CDCl_3$) δ 142.31, 139.59, 139.00, 136.73, 134.95, 134.76, 134.23, 128.28, 126.47, 124.73, 122.31, 120.47, 118.47, 115.64, 112.81, 109.98, 89.83. **HRMS [M+H]+** Calculated: 423.9834 ($C_{20}H_{11}INO_2$); Found:423.9822.

Synthesis of 3-(4,4,5,5-tetramethyl-1,3,2-dioxaborolan-2-yl)quinolino[3,2,1-de]acridine-5,9-dione (3)

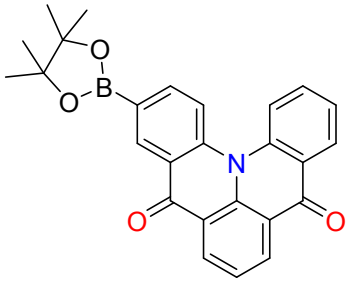

Compound **2** (4.2 g, 10 mmol, 1 equiv.), bis(pinacolato)diboron (3.3 g, 13 mmol, 1.3 equiv.), $Pd(dppf)Cl_2$ (366 mg, 0.5 mmol, 0.05 equiv.) and KOAc (3.0 g, 30 mmol, 3 equiv.) were dissolved in *N,N*-dimethylformamide (50 mL), and were heated to 100 °C under a nitrogen atmosphere for 6 h. The mixture was cooled to room temperature and then filtered through Celite. The organic phase was collected and concentrated under reduced pressure. The crude product was purified by silica gel column chromatography (hexane: ethyl acetate = 5:1) to afford the desired product as a yellow solid. **Yield**: 87% (3.68 g). **R_f**: 0.26 (hexane: ethyl acetate=5:2). **Mp**: 272-273 °C. **^{1}H NMR** (500 MHz, CD_2Cl_2) δ 8.81 (d, *J* = 1.5 Hz, 1H), 8.70 – 8.65 (m, 2H), 8.42 (dd, *J* = 7.9, 1.6 Hz, 1H), 8.11 (dd, *J* = 8.5, 5.8 Hz, 2H), 8.04 (dd, *J* = 8.5, 1.6 Hz, 1H), 7.71 (ddd, *J* = 8.7, 7.2, 1.6 Hz, 1H), 7.64 (t, *J* = 7.6 Hz, 1H), 7.52 – 7.48 (m, 1H), 1.38 (s, 12H). **HRMS [M+H]+** Calculated: 424.1720 ($C_{26}H_{23}BNO_4$); Found:424.1710.

Synthesis of [3,3'-biquinolino[3,2,1-de]acridine]-5,5',9,9'-tetraone (DDiKTa)

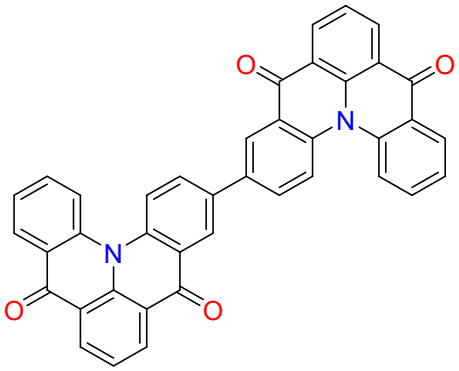

Compound **2** (0.85 g, 2 mmol, 1 equiv.), compound **3** (0.85 g, 2 mmol, 1 equiv.), $Pd(PPh_3)_4$ (116 mg, 0.1 mmol, 0.05 equiv.), 2M Na_2CO_3 (2 mL) and THF (50 mL) were combined under a nitrogen atmosphere. The reaction mixture was heated to reflux and stirred for 12 h. The reaction mixture was cooled to room temperature and the product was filtered and washed with water (3 × 50 mL) and THF (3 × 30 mL) to afford the desired product as a yellow solid. **Yield**: 65% (0.77 g). $\mathbf{R_f}$: 0.31 (hexane: ethyl acetate = 5:2). **Mp**: >400 °C. **^{1}H NMR** (400 MHz, Chloroform-*d*) δ 8.94 (d, *J* = 6.5 Hz, 3H), 8.65 – 8.55 (m, 1H), 8.44 (d, *J* = 8.8 Hz, 1H), 8.31 (dd, *J* = 8.5, 5.3 Hz, 2H), 7.88 (dt, *J* = 23.0, 7.7 Hz, 2H), 7.69 (t, *J* = 7.5 Hz, 1H). **^{13}C NMR** (101 MHz, Chloroform-*d*) δ 139.77, 139.60, 139.12, 138.88, 136.07, 135.02, 134.74, 134.24, 132.34, 128.27, 126.54, 125.75, 124.73, 121.91, 120.73, 118.49, 115.66, 112.83, 110.00.

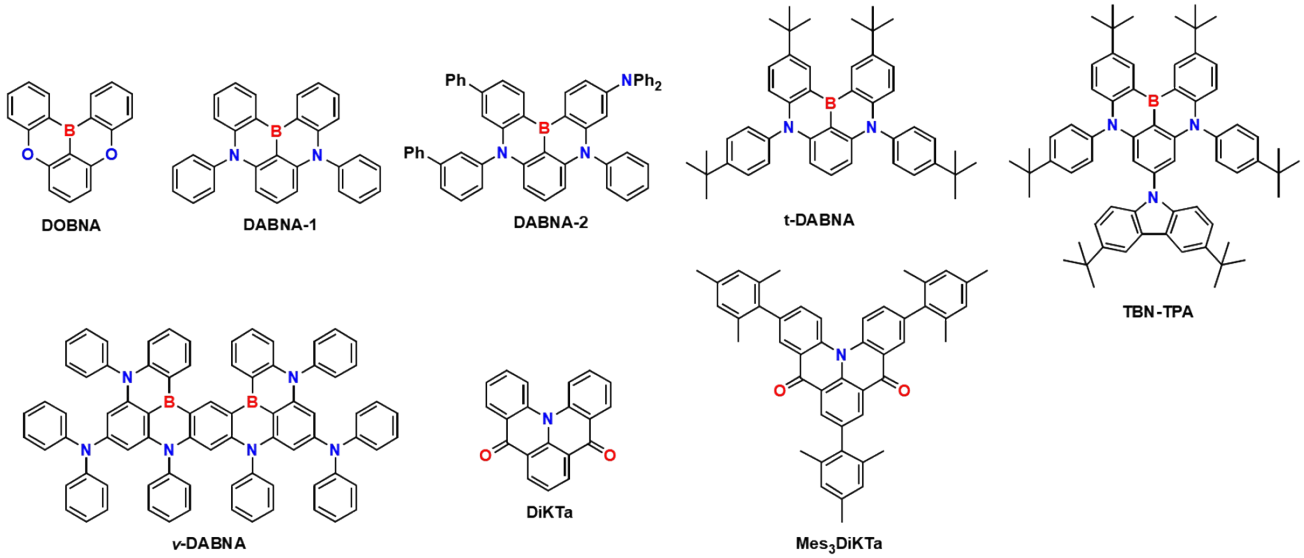

Figure S1. Chemical structures of previously reported MR TADF emitters.

Theoretical calculations

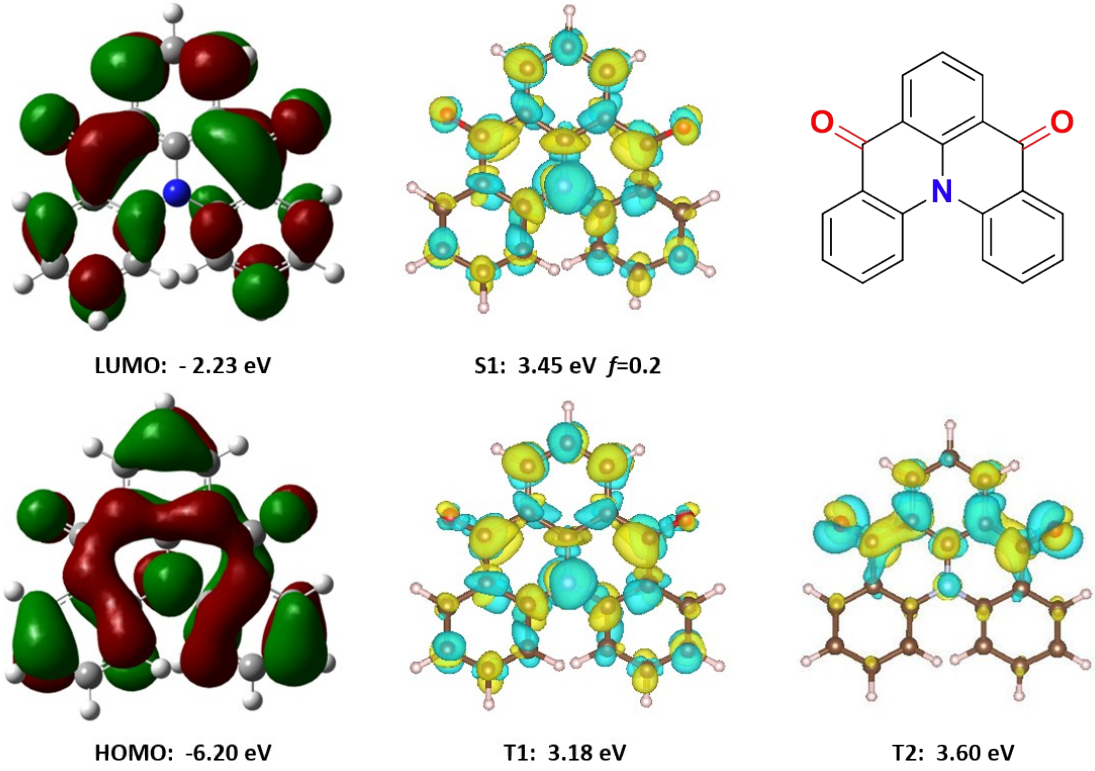

Figure S2. Molecular orbitals energy and isocontour plots (cutoff=0.02 a.u.) in the gas phase obtained at PBE0/6-31G(d,p) level (*top* and *bottom left*. Difference density plots with respect to the gas phase ground state for S_1, T_1 and T_2 excited states for **DiKTa** calculated at SCS-CC2/cc-pVDZ level. *f* indicates the oscillator strength.

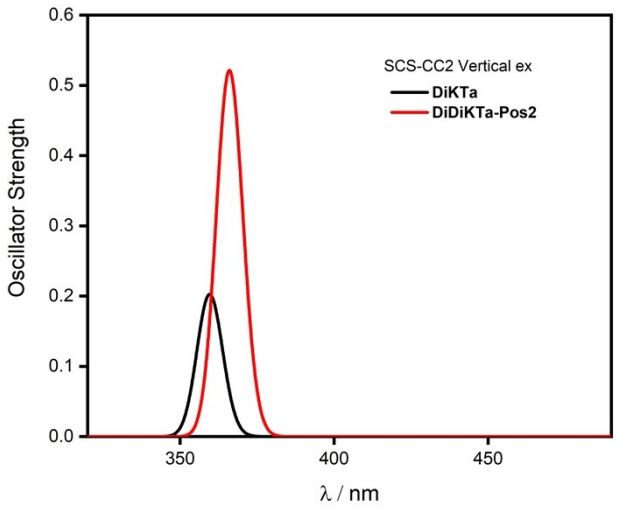

Figure S3. Simulated absorption spectra for **DiKTa** and **DDiKTa** based on SCS-CC2/cc-pVDZ. The y-axis intensity scale indicates the oscillator strength.

The computationally predicted fluorescence rate (k_f), where *f* is oscillator strength (unitless) and ΔE is vertical energy (cm^{-1}) is calculated according.[17]

$$k_f = \frac{f\Delta E^2}{1.499}$$

Table S1. Calculated vertical excited states properties of **DiKTa** obtained using SCS-CC2/cc-pVDZ in the gas phase.

Excited state	**Energy / eV**	***f***	**single electron contribution / %**	**Nature**	**Charge Transferred**	**DCT**	**Overlap integral**	k_f **/ × 10^{-8} s^{-1}**
T_1	3.18		97.22	H→L 82% H3→L 5% H5→L1 3% H8→L 2%	0.592	0.606	0.99	N/A
S_1	3.45	0.20	88.49	H→L 86% H2→L3 3%	0.591	0.812	0.98	N/A
T_2	3.60		98	H2→L 21% H5→L 17% H→L1 16% H7→L 11% H6→L1 6% H2→L4 5% H1→L3 4% H4→L 3% H3→L3 2% H1→L3 2%	0.483	0.242	0.98	1.05

Where H = HOMO, H1 = HOMO -1, H2 = HOMO -2, H3 = HOMO -3, H4 = HOMO -4, H5 = HOMO -5, H6 = HOMO -6, L = LUMO, L1 = LUMO +1, L2 = LUMO +2, L3 = LUMO +3, CT = charge transferred, DCT = distance of charge transferred, *f* = oscillator strength

Table S2. Calculated vertical excited states properties of **DDiKTa** obtained using SCS-CC2/cc-pVDZ in the gas phase.

Excited state	**Energy / eV**	***f***	**single electron contribution / %**	**Transition**	**CT**	**DCT**	**Overlap integral**	k_f / × 10^{-8} s^{-1}
T1	3.12		97.23	H→L1 48% H1→L 29% H→L2 3% H6→L2 2%	0.545	0.335	0.99	N/A
T2	3.13		97.14	H→L 49% H1→L1 33% H6→L 2% H2→L 2%	0.577	0.405	0.99	N/A
S1	3.39	0.52	88.5	H→L1 52% H1→L 33% H2→L1 2%	0.582	0.473	0.98	2.600
S2	3.39	0.01	88.47	H→L 53% H1→L1 32% H2→L 2%	0.572	0.519	0.98	0.457

Where H = HOMO, H1 = HOMO -1, H2 = HOMO -2, H6 = HOMO -6, L = LUMO, L1 = LUMO +1, L2 = LUMO +2, CT = charge transferred, DCT = distance of charge transferred, *f* = oscillator strength

Photophysical characterization

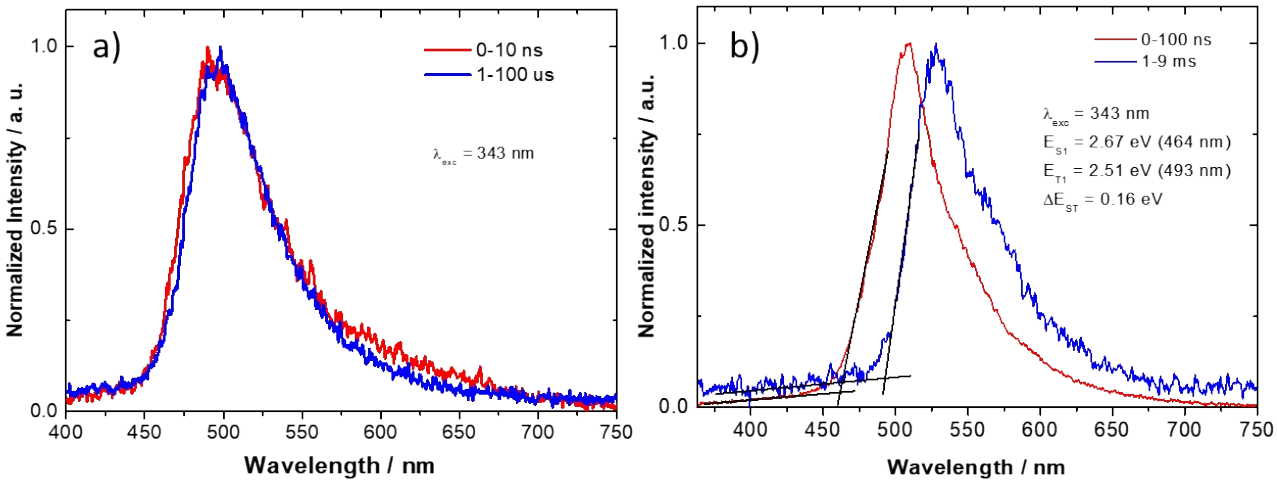

Figure S4. Time-resolved spectra of 9 wt% **DDiKTa** dispersed in DPEPO matrix; a) prompt emission (0 ns delay and 10 ns integration time) and delayed fluorescence (1μs delay and 100 μs integration time) at room temperature; b) Prompt fluorescence (0 ns delay and 100 ns integration time) and phosphorescence spectrum (1 ms delay and 100 ms integration time) at 77 K. λ_{exc} = 343 nm.

Table S3. Electrochemical data and theoretical properties of **DDiKTa** and **DiKTa**

	Electrochemical potential [a]			Theoretical [e]			
	E_{ox} [b] / V	E_{red} [c] / V	ΔE [d] / V	HOMO / eV	LUMO / eV	f [f]	ΔE_{ST} / eV
DDiKTa	1.63	-1.27	2.90	-6.04	-2.34	0.52	0.27
DiKTa	1.65	-1.33	2.98	-6.20	-2.23	0.20	0.27

[a] Potential values were obtained from the DPV peak values and referenced with respect to SCE (Fc/Fc^+ = 0.46 eV), the measurement of DDiKTa was performed in DCM while the measurement of DiKTa was performed in MeCN;[18] [b] Oxidation potential calculated from the DPV peak value; [c] Reduction potential calculated from the DPV peak value; [d] $\Delta E = E_{ox}-E_{red}$; [e] Calculated in the gas phase at SCS-CC2/cc-pVDZ level; [f] Calculated oscillator strength of S_1.

Table S4. Optoelectronic properties of **DDiKTa** and **DiKTa**

	In toluene						In film [g]			
	λ_{abs} [a] / nm	ε / $\times 10^{-3}$ M^{-1} cm^{-1}	λ_{PL} [b] / nm	Φ_{PL} [c] / %	ΔE_{ST} [d] / eV	FWHM[e] / nm/cm^{-1}	λ_{PL} / nm	Φ_{PL} [f] / %	ΔE_{ST} / eV	FWHM / nm/cm^{-1}
DDiKTa	444	10.4	470	29	0.21	47/1639	490	72	0.16	61/2434
DiKTa[18]	435	21	453	26	0.20	27/1251	470	16	0.20	43/1857

[a] UV–vis absorption of CT transition; [b] PL in toluene degassing with N_2; [c] Photoluminescence quantum yield in toluene relative to quinine sulfate in 1N H_2SO_4 (Φ_{PL} = 54.6%);[11] [d] Energy gap between S_1 and T_1 calculated from the difference of the onsets of the fluorescence and phosphorescence spectra in toluene glass at 77 K; [e] Full wavelength at half maximum; [f] Obtained using an integrating sphere under N_2; [g] 9 wt% **DDiKTa** doped in DPEPO, 10wt% DiKTa doped in mCP.

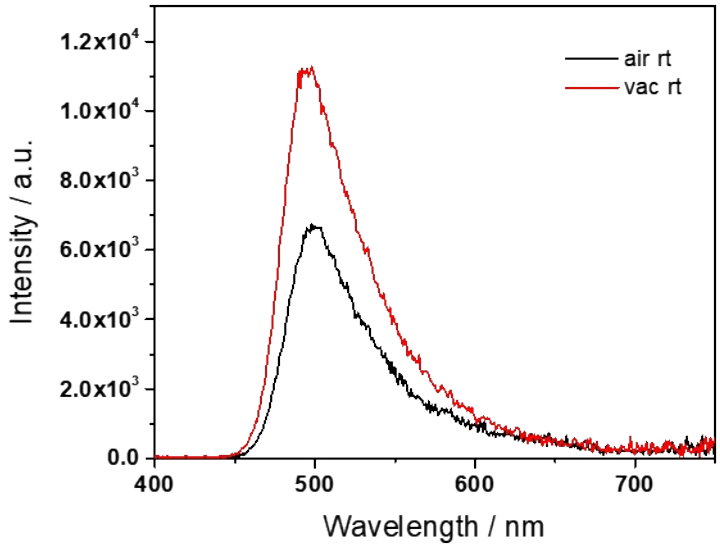

Figure S5. Comparison of steady-state PL spectra of 9 wt% **DDiKTa** dispersed in DPEPO matrix at room temperature under N_2 and air. λ_{exc} = 330 nm.

Table S5. Transient PL decay data of 9 wt% **DDiKTa** dispersed in DPEPO matrix at various temperature

T / K	τ1 / ns	τ2 / ns	A1	A2	Rel%-1 / %	Rel%-2 / %
300	7.25	1168.9	13566	105	44	56
250	7.54	1163.9	14123	105	46	54
200	7.56	1125.7	15677	97	52	48
150	7.70	1083.3	16416	106	50	50
77	8.22	1001.2	15568	112	49	51

Table S6. Photophysical properties and calculated rate constants of 9 wt% **DDiKTa** dispersed in DPEPO matrix at various temperature

T / K	ϕ_{PL} / %	φ_f / %	φ_d / %	k_f / s^{-1}	k_d / s^{-1}	k_rS / s^{-1}	k_{ISC} / s^{-1}	k_{RISC} / s^{-1}	k_{nrT} / s^{-1}
300	72%	32%	40%	4.41E+07	3.42E+05	1.41E+07	3.00E+07	6.30E+05	1.41E+05
280	67%	30%	37%	4.22E+07	3.35E+05	1.28E+07	2.94E+07	5.83E+05	1.59E+05
260	66%	31%	35%	4.06E+07	3.03E+05	1.24E+07	2.82E+07	5.02E+05	1.49E+05
240	64%	32%	32%	4.39E+07	3.00E+05	1.43E+07	2.96E+07	4.39E+05	1.58E+05
220	63%	33%	30%	4.64E+07	2.79E+05	1.56E+07	3.08E+07	3.70E+05	1.55E+05
210	61%	33%	28%	4.66E+07	2.50E+05	1.56E+07	3.10E+07	3.18E+05	1.44E+05

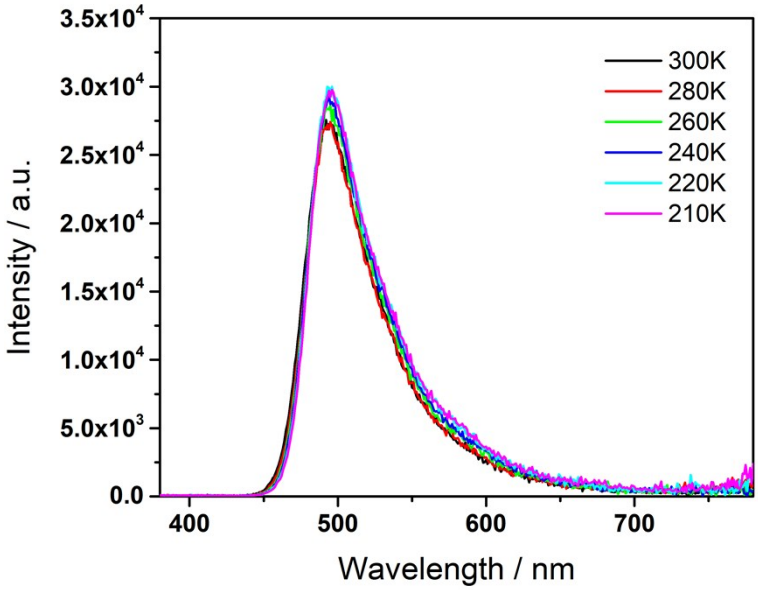

Figure S6. Temperature dependent steady state PL spectra of 9 wt% **DDiKTa** in DPEPO (λ_{exc} = 330 nm)

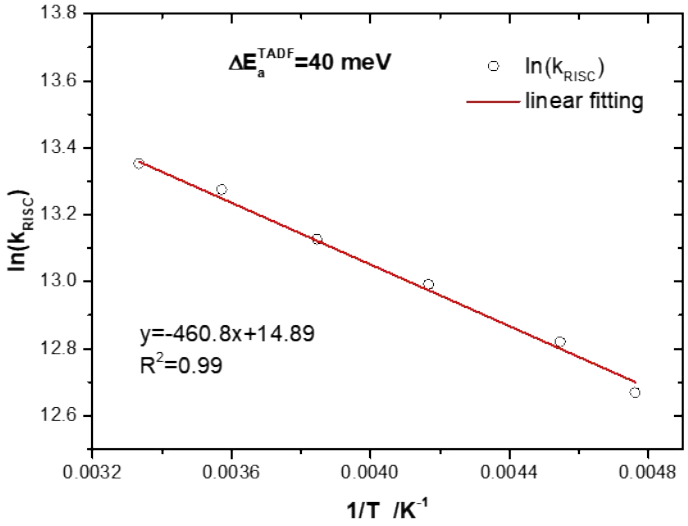

Figure S7. Arrhenius plot of 9 wt% **DDiKTa** in DPEPO

Table S7. Summary of solvatochromic PL properties of **DDiKTa**

Solvent	λ_{PL} [a]	FWHM [b]
	nm	nm / cm-1
Hexane (Hex)	457	32 / 1514
Toluene (Tol)	466	38 / 1701
Diethyl ether (Et_2O)	462	36 / 1646
Ethyl acetate (EA)	472	44 / 1929
THF	474	44 / 1929
$CHCl_3$	479	43 / 1843

[a] Peak value of PL spectra obtained under aerated conditions at 298 K, concentration 2.3×10^{-5} M, λ_{exc} = 330 nm. [b] Full wavelength at half maximum of corresponding PL spectra

NMR spectra

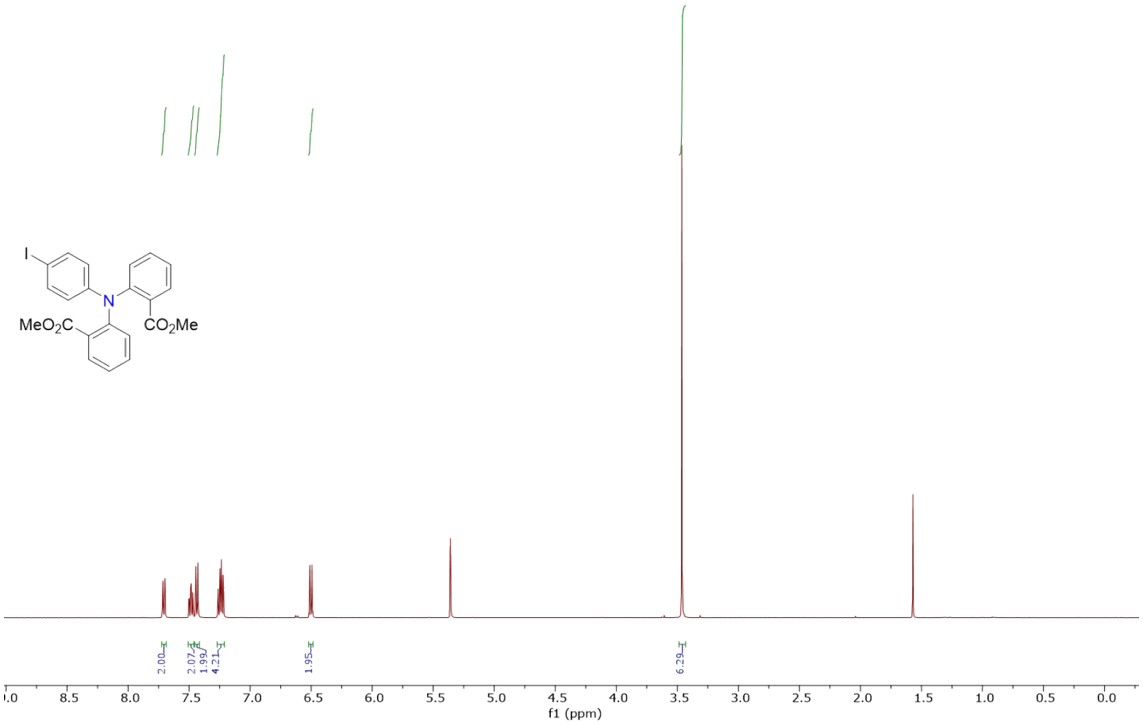

Figure S7. ^{1}H NMR of **dimethyl 2,2'-((4-iodophenyl)azanediyl)dibenzoate (1)**

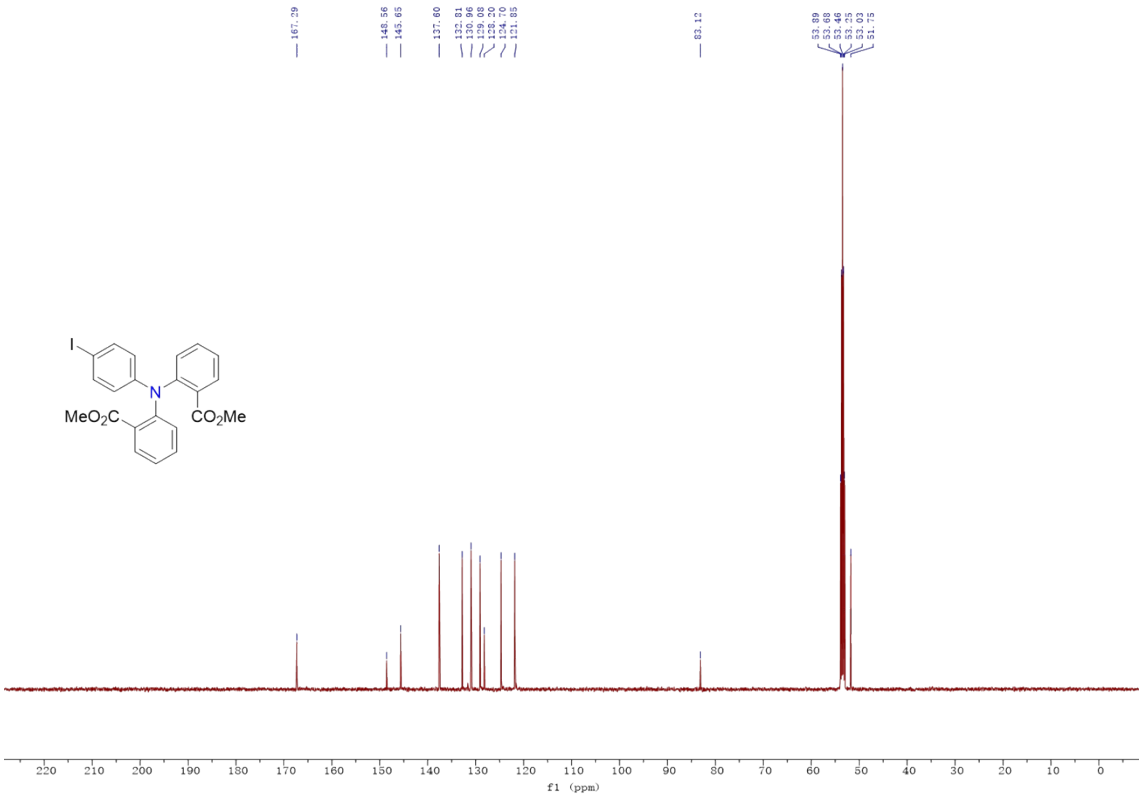

Figure S8. ^{13}C NMR of **dimethyl 2,2'-((4-iodophenyl)azanediyl)dibenzoate (1)**

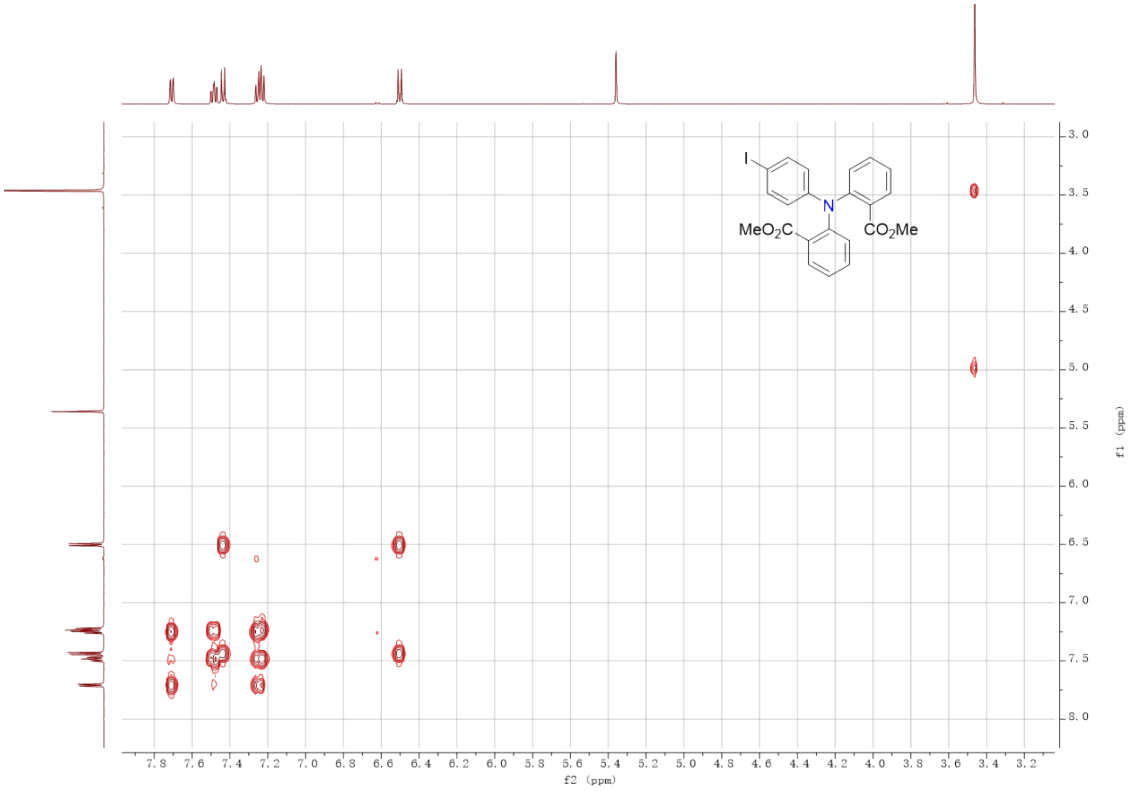

Figure S9. 2D ^{1}H-^{1}H COSY NMR of **dimethyl 2,2'-((4-iodophenyl)azanediyl)dibenzoate (1)**

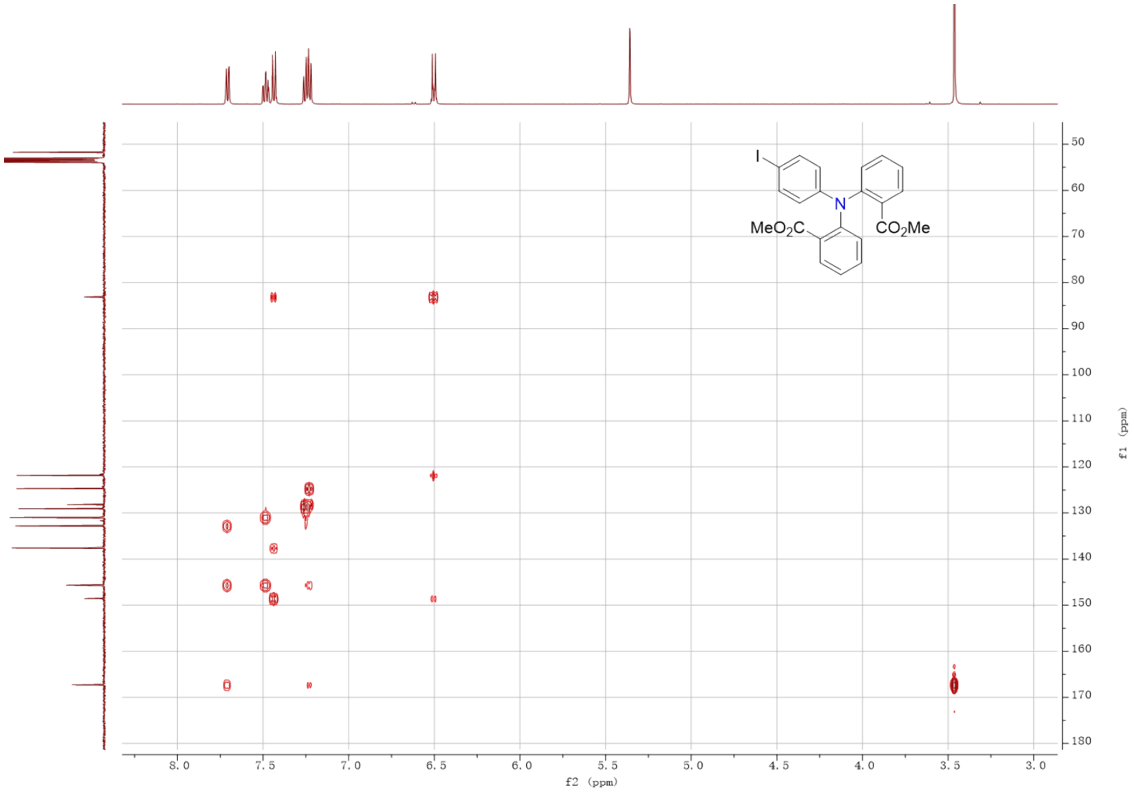

Figure S10. 2D ^{1}H-^{13}C HSQC NMR of **dimethyl 2,2'-((4-iodophenyl)azanediyl)dibenzoate (1)**

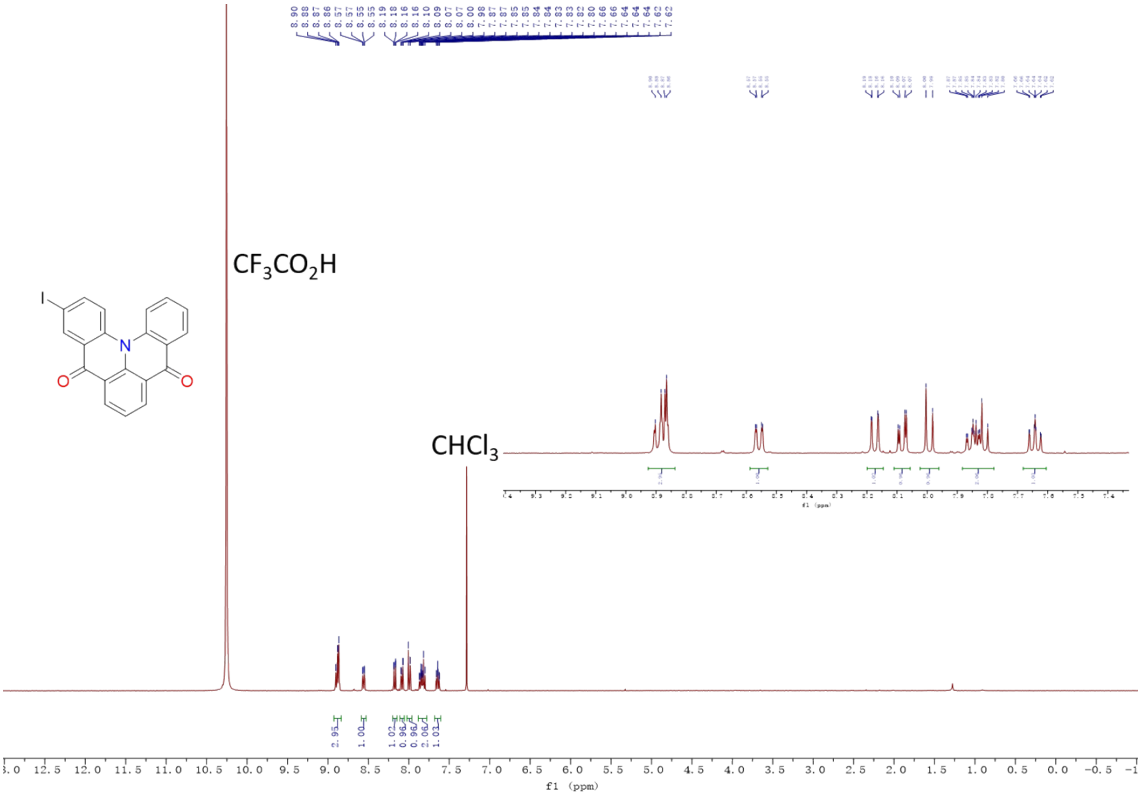

Figure S11. ^{1}H NMR of **3-iodoquinolino[3,2,1-de]acridine-5,9-dione (2)** (a drop of Trifluoroacetic acid was added in $CDCl_3$ to improve the solubility)

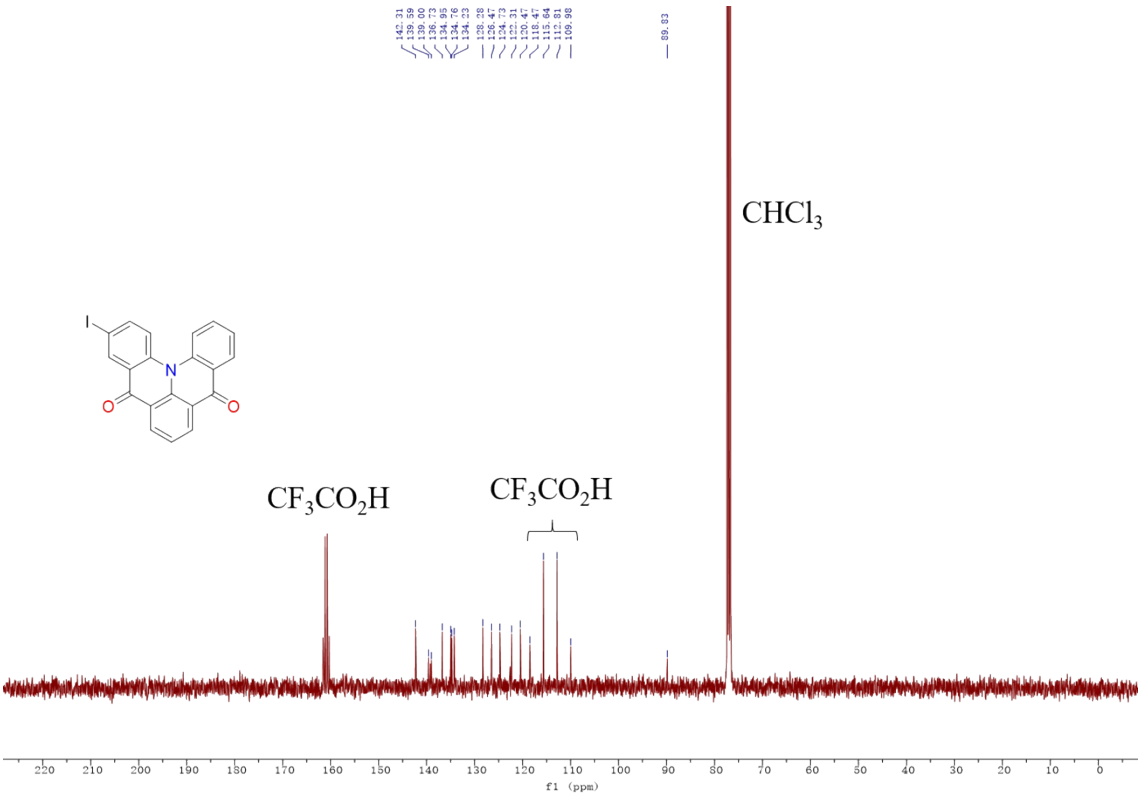

Figure S12. ^{13}C NMR of **3-iodoquinolino[3,2,1-de]acridine-5,9-dione (2)** (a drop of Trifluoroacetic acid was added in $CDCl_3$ to improve the solubility)

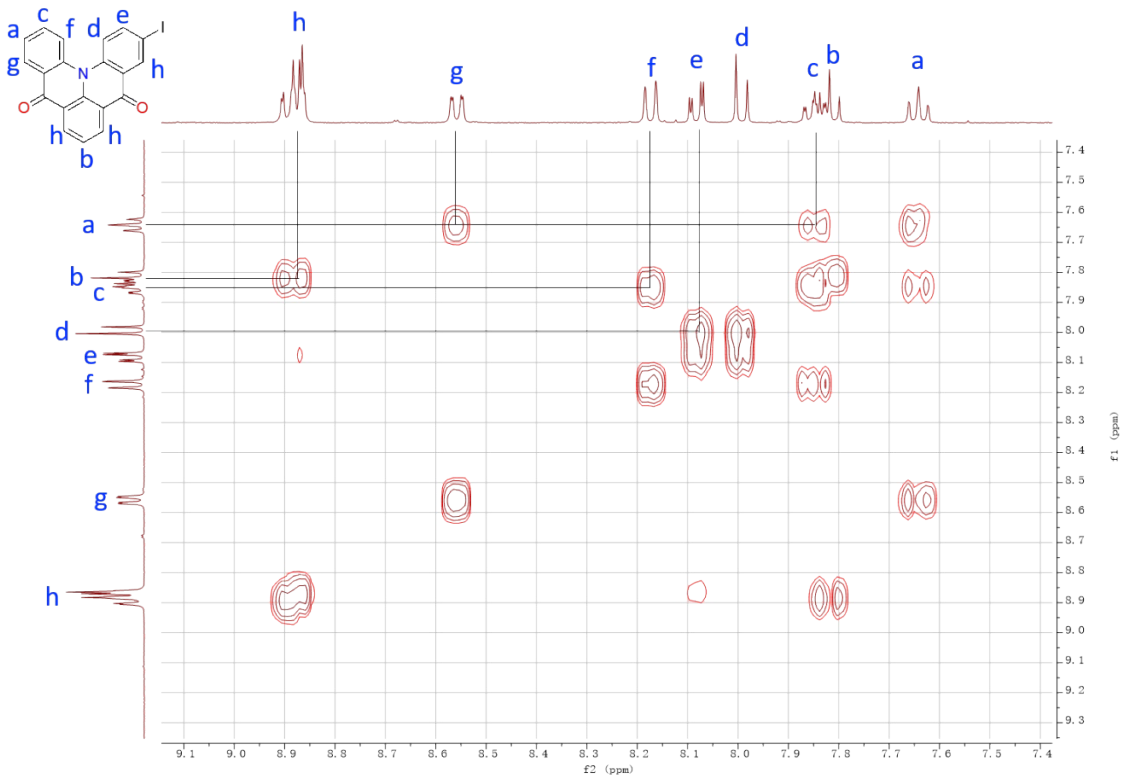

Figure S13. 2D ^{1}H-^{1}H COSY NMR of **3-iodoquinolino[3,2,1-de]acridine-5,9-dione (2)** (a drop of Trifluoroacetic acid was added in $CDCl_3$ to improve the solubility)

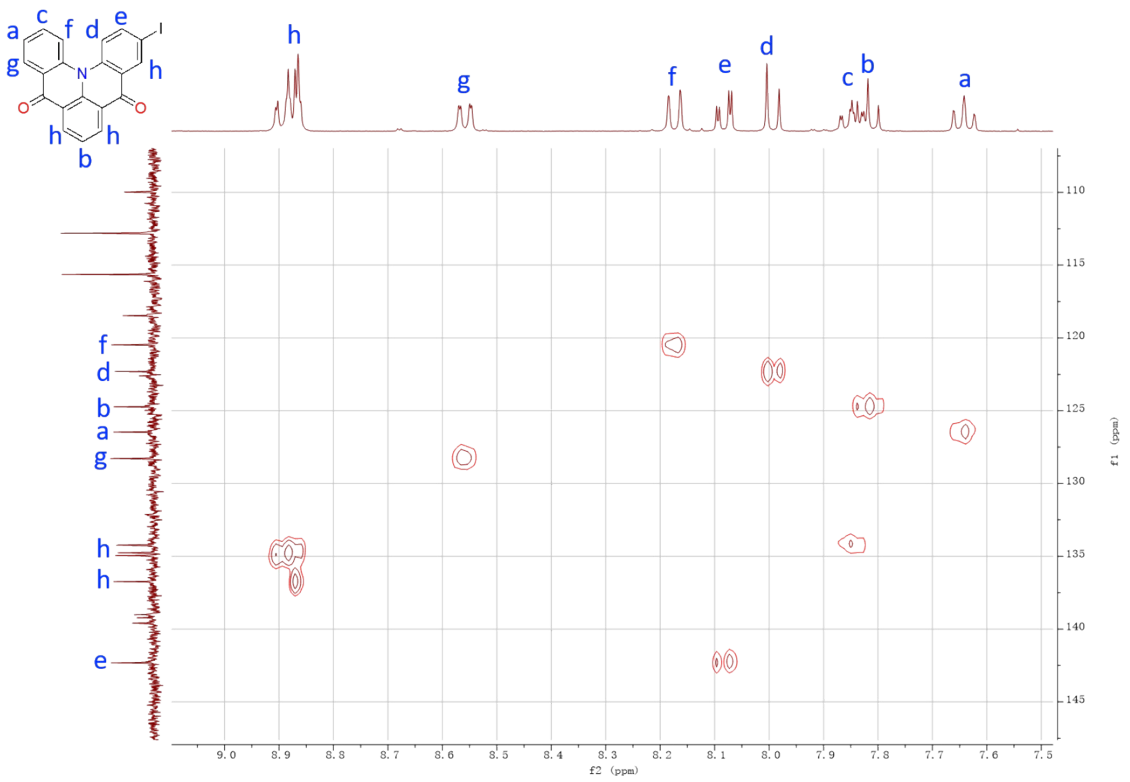

Figure S14. 2D ^{1}H-^{13}C HSQC NMR of **3-iodoquinolino[3,2,1-de]acridine-5,9-dione (2)** (a drop of Trifluoroacetic acid was added in $CDCl_3$ to improve the solubility)

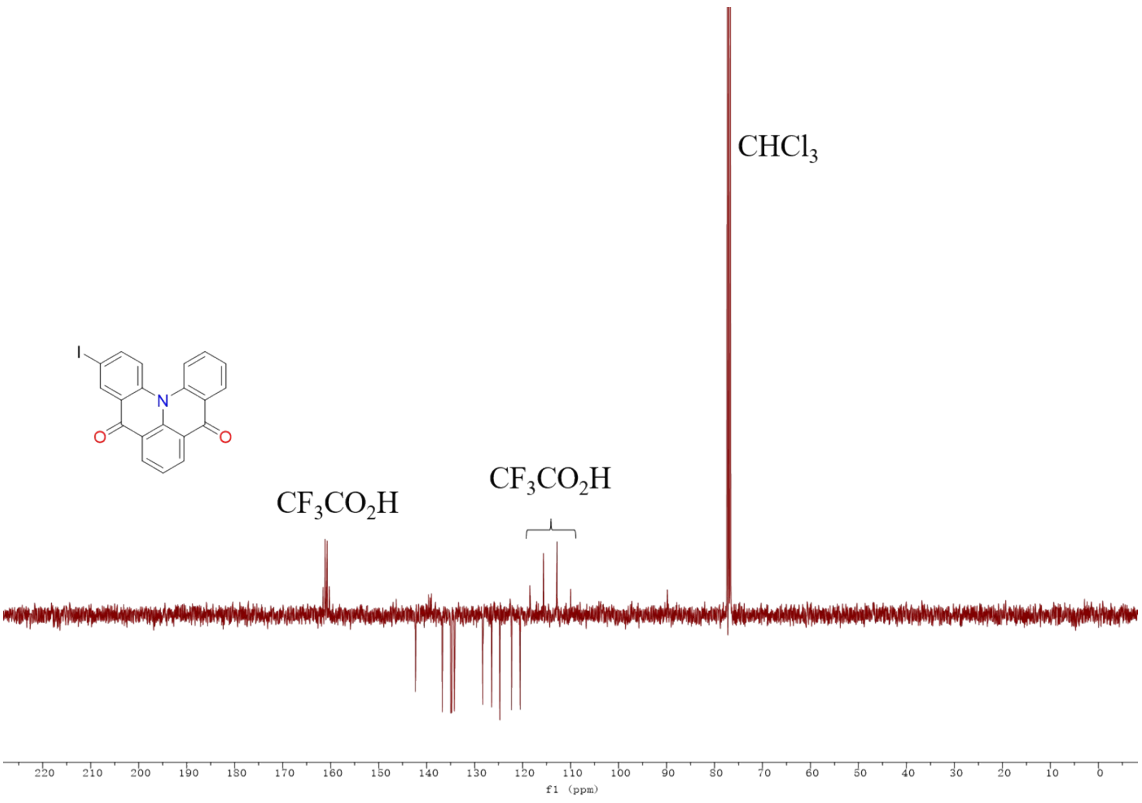

Figure S15. DEPTQ NMR of **3-iodoquinolino[3,2,1-de]acridine-5,9-dione (2)** (a drop of Trifluoroacetic acid was added in $CDCl_3$ to improve the solubility)

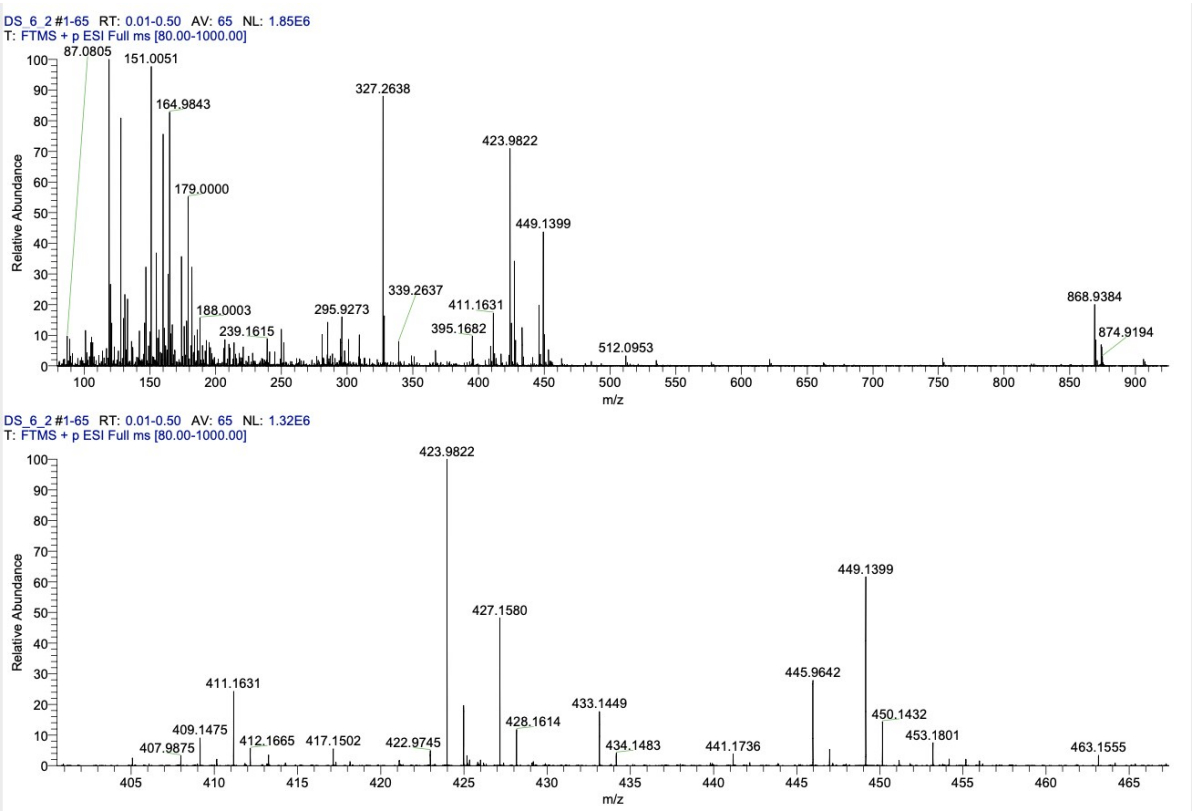

Figure S16. HRMS of **3-iodoquinolino[3,2,1-de]acridine-5,9-dione (2)**

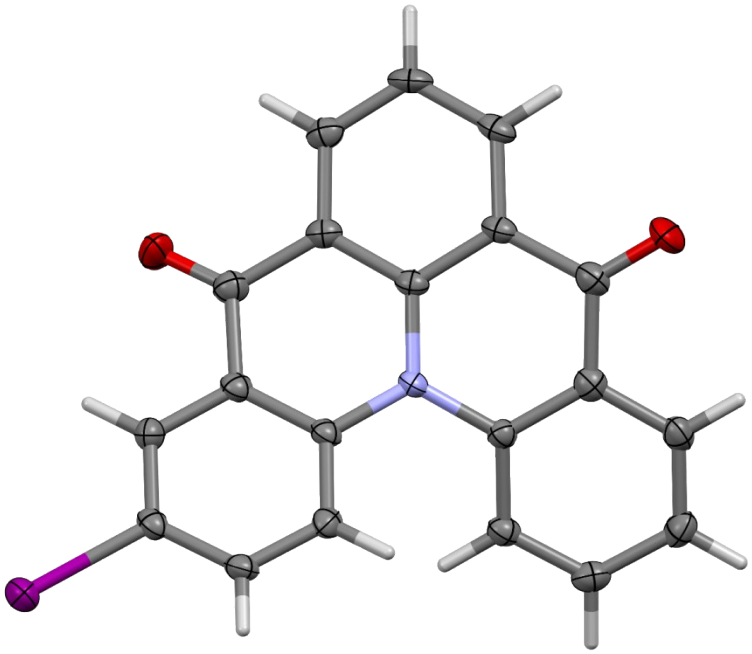

Figure S17. Thermal ellipsoid diagram of the X-ray structure of compound **2**. Ellipsoids are drawn at the 50% probability level.

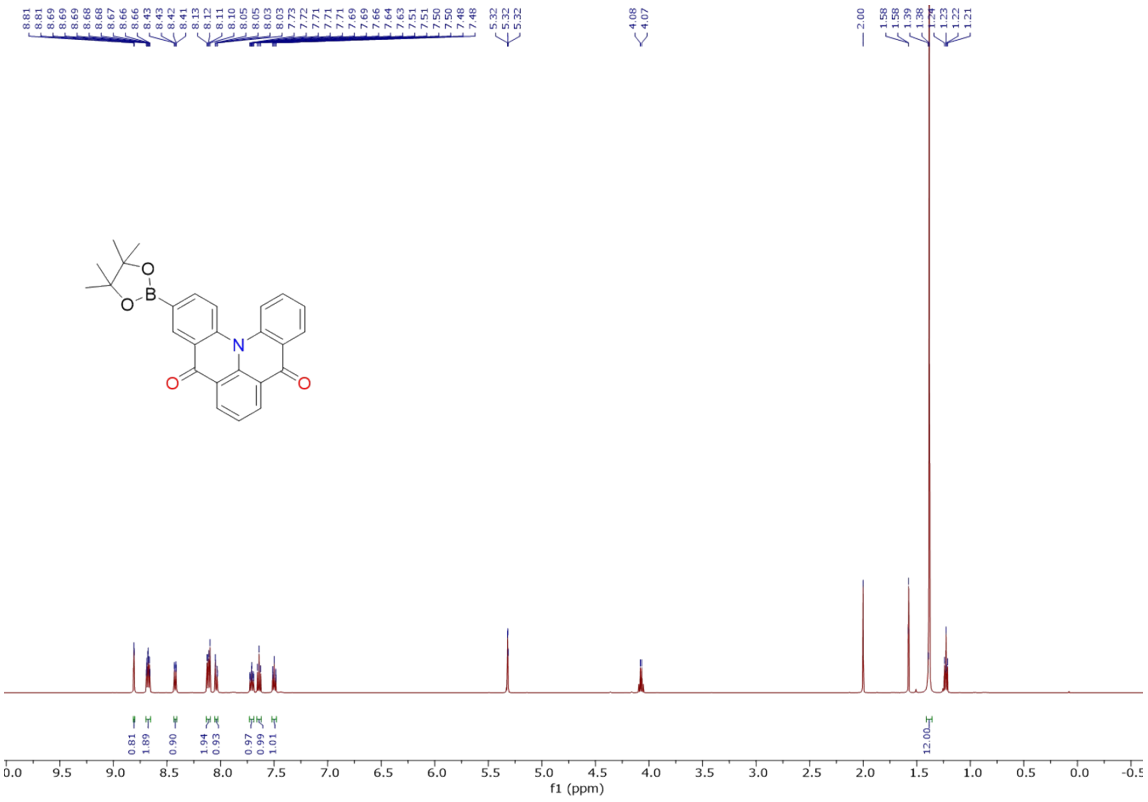

Figure S18. ^{1}H NMR of **3-(4,4,5,5-tetramethyl-1,3,2-dioxaborolan-2-yl)quinolino[3,2,1-de]acridine-5,9-dione (3)**

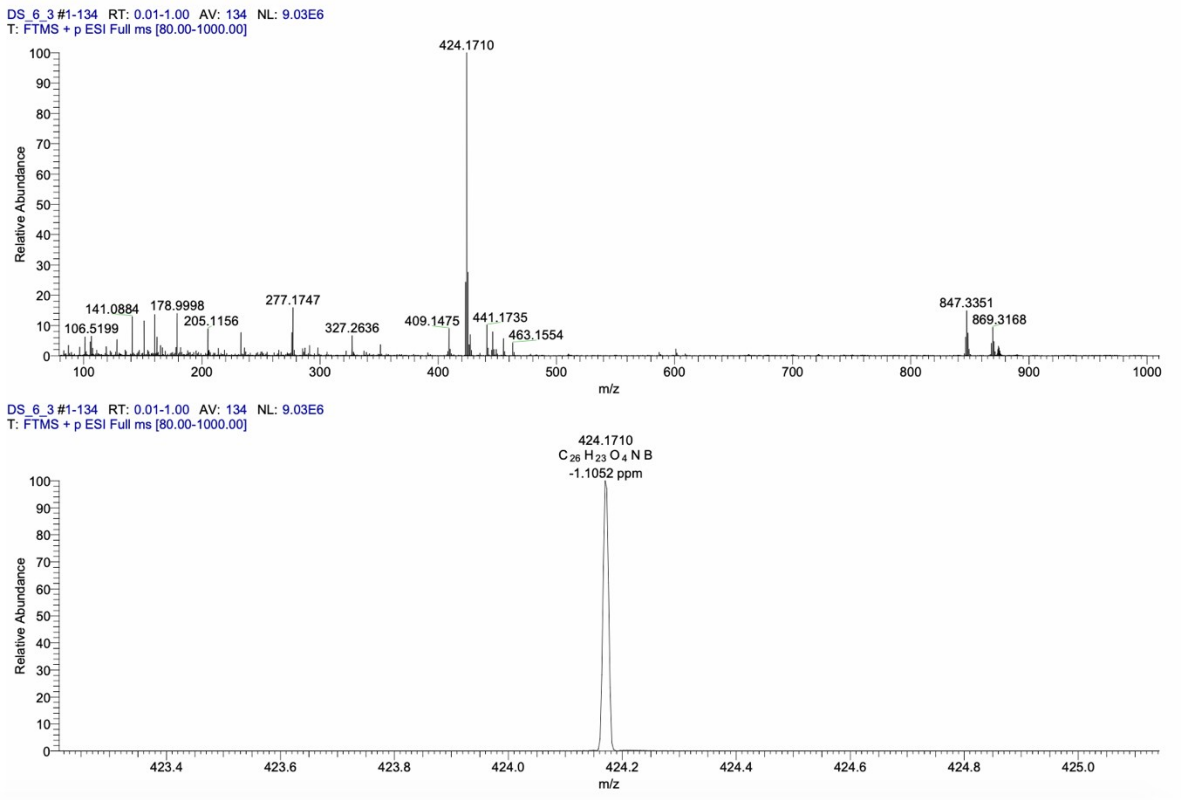

Figure S19. HRMS of **3-(4,4,5,5-tetramethyl-1,3,2-dioxaborolan-2-yl)quinolino[3,2,1-de]acridine-5,9-dione (3)**

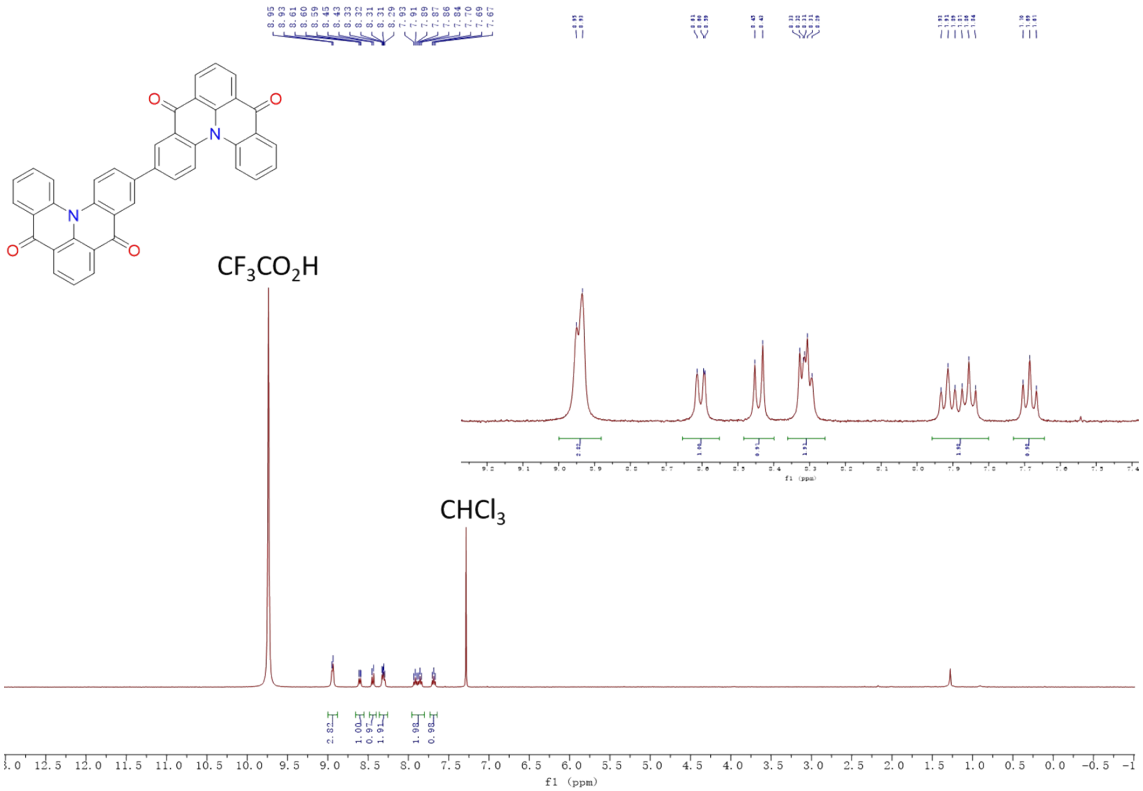

Figure S20. ^{1}H NMR of **[3,3'-biquinolino[3,2,1-de]acridine]-5,5',9,9'-tetraone (DDiKTa)** (a drop of Trifluoroacetic acid was added in $CDCl_3$ to improve the solubility)

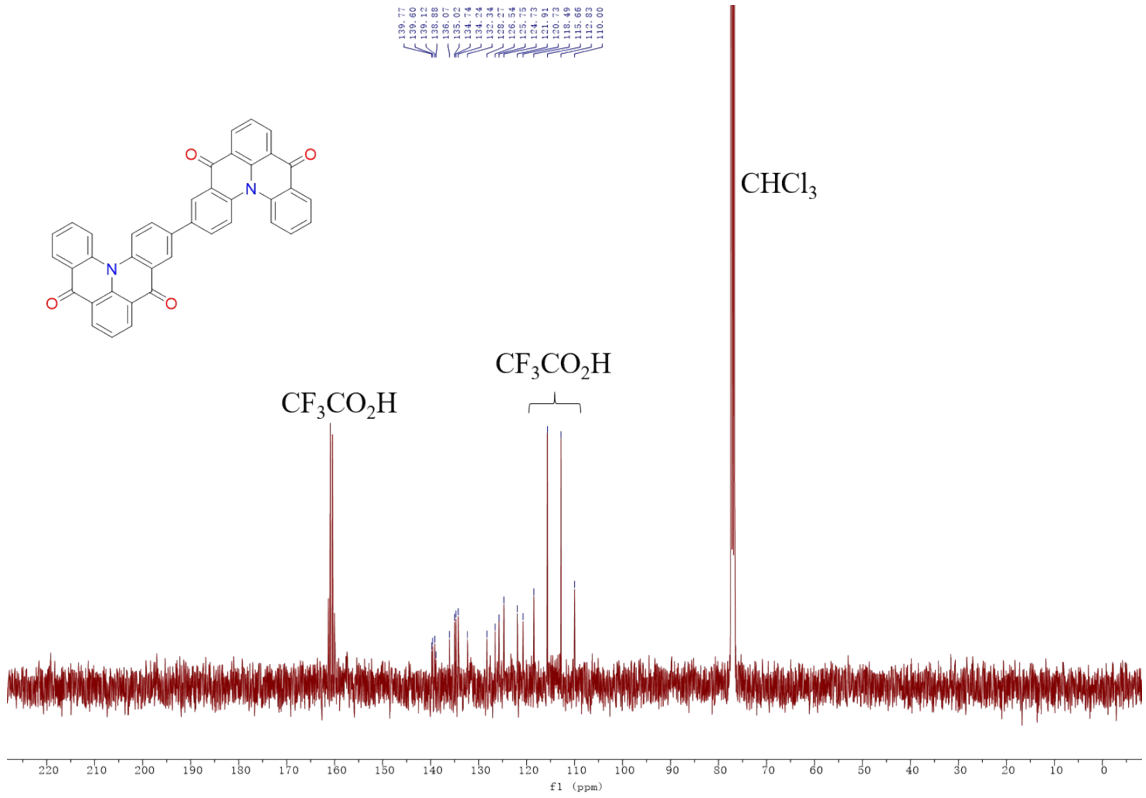

Figure S21. ^{13}C NMR of **[3,3'-biquinolino[3,2,1-de]acridine]-5,5',9,9'-tetraone (DDiKTa)** (a drop of Trifluoroacetic acid was added in $CDCl_3$ to improve the solubility)

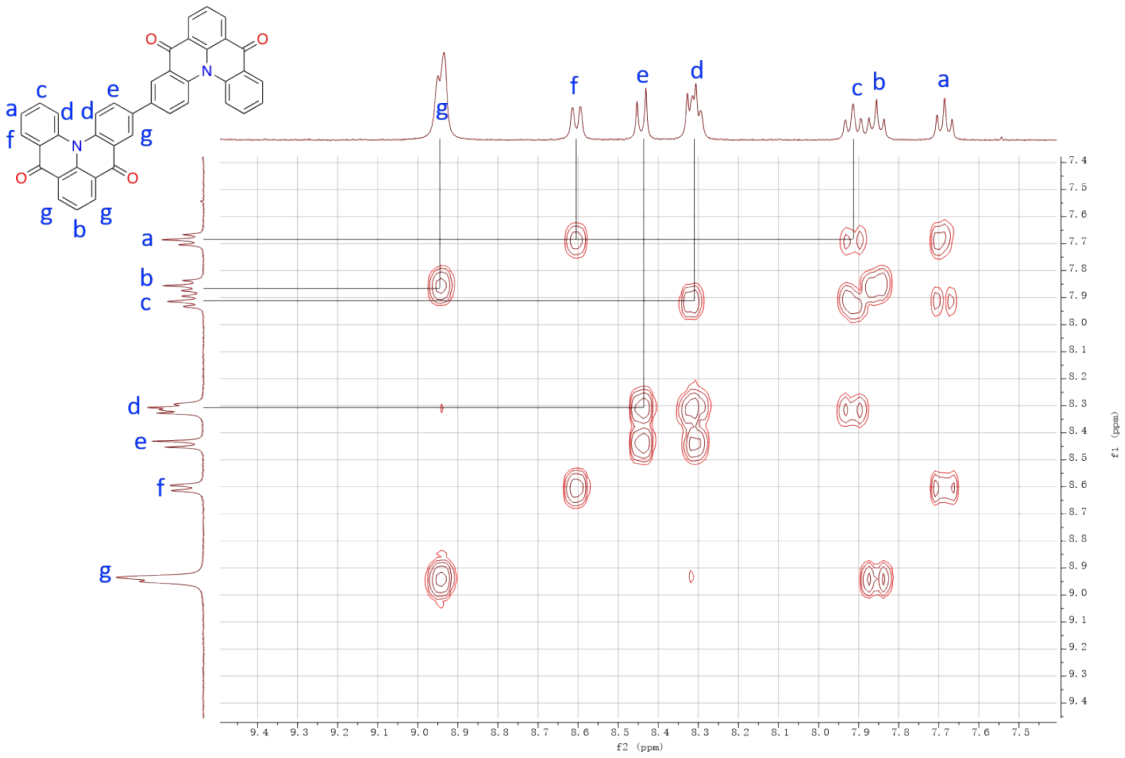

Figure S22. 2D ^{1}H-^{1}H COSY NMR of **[3,3'-biquinolino[3,2,1-de]acridine]-5,5',9,9'-tetraone (DDiKTa)** (a drop of Trifluoroacetic acid was added in $CDCl_3$ to improve the solubility)

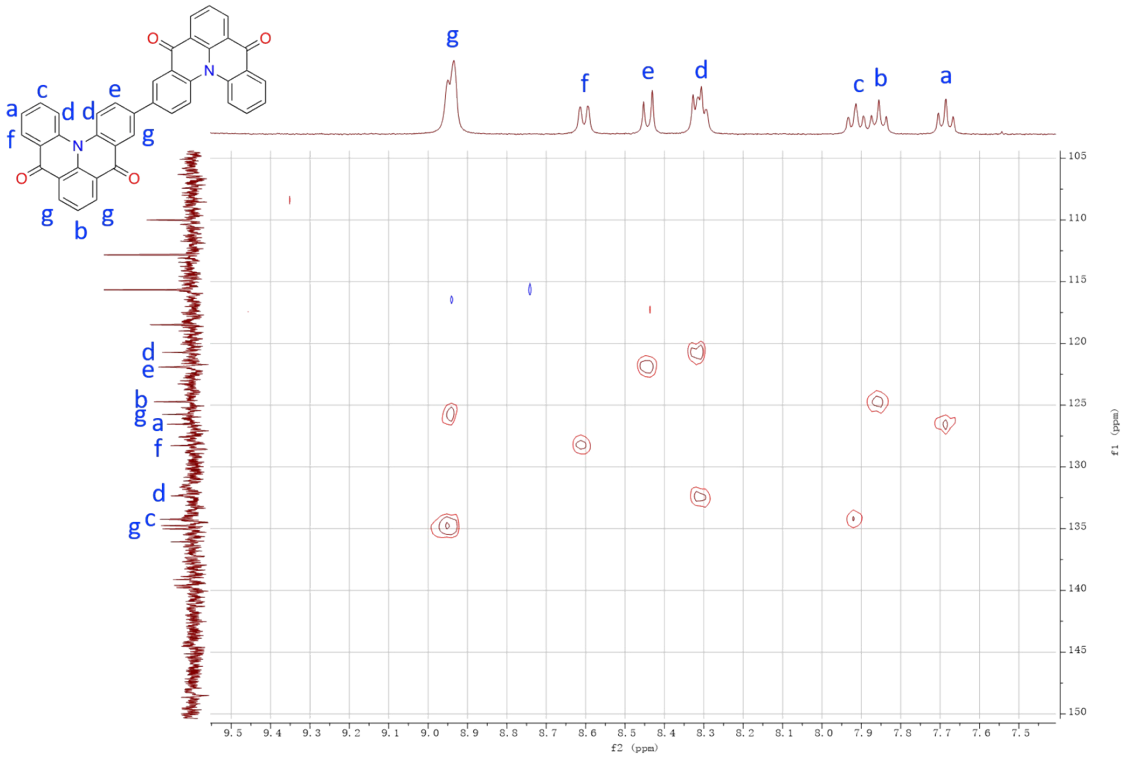

Figure S23. 2D ^{1}H-^{13}C HSQC NMR of **[3,3'-biquinolino[3,2,1-de]acridine]-5,5',9,9'-tetraone (DDiKTa)** (a drop of Trifluoroacetic acid was added in $CDCl_3$ to improve the solubility)

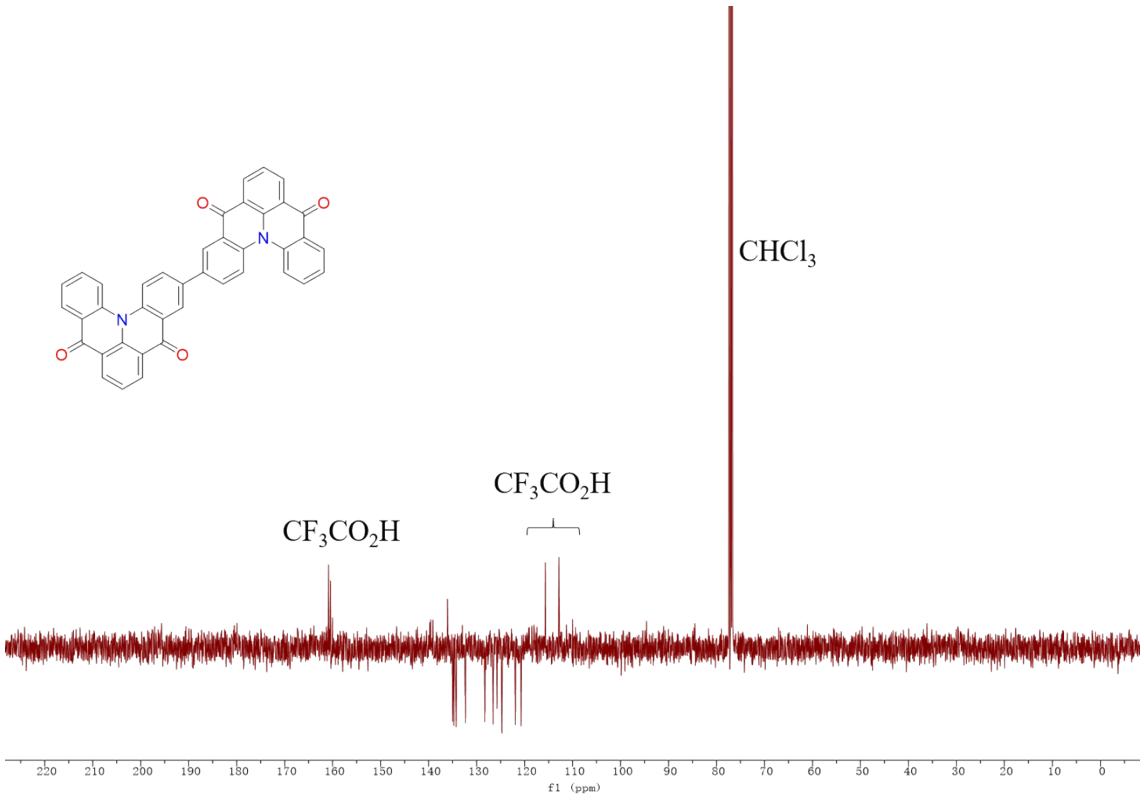

Figure S24. DEPTQ NMR of **[3,3'-biquinolino[3,2,1-de]acridine]-5,5',9,9'-tetraone (DDiKTa)** (a drop of Trifluoroacetic acid was added in $CDCl_3$ to improve the solubility)

Coordinates of DDiKTa calculated using SCS-CC2 / ccpVDZ in the gas phase.

4.95793534735043	13.43771405076456	-4.41358069043075	c
5.41239476497736	10.90431717048721	-3.77197811401312	c
2.79653034757396	14.64768869214191	-3.46249145832795	c
3.72342798247889	9.55838119692992	-2.21241602284050	c
7.08123985753156	9.89144515566811	-4.45722143225433	h
1.09964884788413	13.36739242988234	-1.85826184563885	c
2.35612319807003	16.61407363452878	-3.93147194541142	h
1.54930531930842	10.79413566933724	-1.22632978221433	c
4.24991774392697	6.86929747769631	-1.60710191583484	c
-1.15102685136586	14.72271794673996	-0.86612563428746	c
-0.13902085832340	9.48736496085910	0.34873184201251	n
2.05101820394880	5.49329516769113	-0.52543731811060	c
6.28129839581124	5.81691206146236	-2.11973410725965	o
-2.40743962144821	13.42479447200228	1.28608043525103	c
-1.81205396780871	16.83249337697617	-1.64358148248113	o
-0.13256146826974	6.80921940815973	0.30343458317480	c
-1.78922928970057	10.89755768445314	1.92897073379755	c
2.08721438273522	2.82465677871551	-0.53363451281147	c
-4.09277789302999	14.81913711515319	2.82502945298110	c
-2.31954934465030	5.38563675301322	0.92669618137643	c
-2.71912163040334	9.88124073939153	4.23000030063786	c
3.81785735415096	1.91849815950419	-1.21649755147382	h
-0.02476311024110	1.40315181845384	0.21073298188407	c
-4.52985689837319	16.75353551679266	2.23785133918125	h
-5.10450324487173	13.76580199776344	5.02272755673042	c
-2.24861272600544	2.74585447350533	0.89358570845288	c
-4.08468782862451	6.34433605853555	1.40237574180269	h
-4.36286399005914	11.30115887513722	5.73949856178318	c
-2.11241720446787	8.01117966898535	4.85909974607781	h
-6.40380436221133	14.85309527922162	6.20943843579473	h

-3.95879273273818	1.69973647071117	1.41096222092302	h
-5.04592019696744	10.48603044683365	7.51568904192719	h
6.27230680515498	14.45758382077353	-5.64263688449788	h
0.02425109559166	-1.40339632538300	0.21070726463520	c
2.24792129133633	-2.74610664283402	0.89413890081594	c
-2.08752516486054	-2.82489336251039	-0.53424389898067	c
2.31884056708336	-5.38588903760450	0.92726406370533	c
3.95797184901888	-1.69999472063165	1.41195503306416	h
-2.05133840910105	-5.49353140223992	-0.52604982792536	c
-3.81797393178365	-1.91872952294544	-1.21759111005442	h
0.13203283221717	-6.80946337063935	0.30335256689201	c
4.08379979878561	-6.34459836443861	1.40359839984236	h
-4.24997970275802	-6.86952987777931	-1.60824717867293	c
0.13850690547606	-9.48760248893055	0.34867595037967	n
-3.72345804607219	-9.55869152887350	-2.21318871516213	c
-6.28115389848461	-5.81708262437850	-2.12157919959283	o
1.78858585506765	-10.89765933957692	1.92916278776815	c
-1.54958458640764	-10.79445240477859	-1.22656222348581	c
-5.41218632823539	-10.90468447950253	-3.77296113751331	c
2.71964911666060	-9.88049637242535	4.22934468084187	c
2.40672313154477	-13.42502448036265	1.28670779324080	c
-1.09999051980626	-13.36781651348168	-1.85809917382897	c
-7.08081650493700	-9.89177152467932	-4.45866602812116	h
-4.95776325347439	-13.43817844978395	-4.41420479540559	c
4.36440646306727	-11.29974217219805	5.73836614081292	c
2.11312587375615	-8.01027787988062	4.85815724438831	h
4.09278239853798	-14.81882241970567	2.82536360711647	c
1.15034663022291	-14.72325005224750	-0.86534143298581	c
-2.79664495748124	-14.64818955985391	-3.46250679738906	c
-6.27192286762588	-14.45808361135206	-5.64345761673535	h
5.04864693242768	-10.48383004231892	7.51374004558772	h
5.10569041101160	-13.76464442838555	5.02211191382951	c

4.52938506962499	-16.75351467828671	2.23879918475277	h
1.81111214522531	-16.83333447494352	-1.64219010964305	o
-2.35629891427453	-16.61467388396090	-3.93112456510911	h
6.40564338730346	-14.85147849135818	6.20852876489953	h

References

1. Connelly, N. G.; Geiger, W. E., Chemical redox agents for organometallic chemistry. *Chem. Rev*. **1996**, *96*, 877-910.
2. Cardona, C. M.; Li, W.; Kaifer, A. E.; Stockdale, D.; Bazan, G. C., Electrochemical Considerations for Determining Absolute Frontier Orbital Energy Levels of Conjugated Polymers for Solar Cell Applications. *Adv. Mater.* **2011,** *23*, 2367-2371.
3. G. W. T. M. J. Frisch, H. B. Schlegel, G. E. Scuseria, M. A. Robb, J. R. Cheeseman, G. Scalmani, V. Barone, B. Mennucci, G. A. Petersson, H. Nakatsuji, M. Caricato, X. Li, H. P. Hratchian, A. F. Izmaylov, J. Bloino, G. Zheng, J. L. Sonnenberg, M. Hada, M. Ehara, K. Toyota, R. Fukuda, J. Hasegawa, M. Ishida, T. Nakajima, Y. Honda, O. Kitao, H. Nakai, T. Vreven, J. A. Montgomery Jr., J. E. Peralta, F. Ogliaro, M. Bearpark, J. J. Heyd, E. Brothers, K. N. Kudin, V. N. Staroverov, R. Kobayashi, J. Normand, K. Raghavachari, A. Rendell, J. C. Burant, S. S. Iyengar, J. Tomasi, M. Cossi, N. Rega, J. M. Millam, M. Klene, J. E. Knox, J. B. Cross, V. Bakken, C. Adamo, J. Jaramillo, R. Gomperts, R. E. Stratmann, O. Yazyev, A. J. Austin, R. Cammi, C. Pomelli, J. W. Ochterski, R. L. Martin, K. Morokuma, V. G. Zakrzewski, G. A. Voth, P. Salvador, J. J. Dannenberg, S. Dapprich, A. D. Daniels, Ö. Farkas, J. B. Foresman, J. V. Ortiz, J. Cioslowski, D. J. Fox, Gaussian Inc., Wallingford, CT: 2013.
4. TURBOMOLE V6.5, 1989-2007, TURBOMOLE GmbH, since 2007; available from http://www.turbomole.com.
5. Adamo, C.; Barone, V., Toward reliable density functional methods without adjustable parameters: The PBE0 model. *J. Chem. Phys.* **1999,** *110*, 6158-6170.
6. Becke, A. D., Dependence of the virial exciton model on basis set and exact-exchange fraction. *J. Chem. Phys.* **2019,** *150*, 241101.
7. R. Dennington, T.Keith; J. Millam, GaussView, Version 5, KS: Semichem Inc.: Shawnee Mission, 2009.
8. Petersson, G.; Al-Laham, M. A., A complete basis set model chemistry. II. Open-shell systems and the total energies of the first-row atoms. *J. Chem. Phys.* **1991**, *94*, 6081-6090.
9. Momma, K.; Izumi, F., VESTA 3 for three-dimensional visualization of crystal, volumetric and morphology data, *J. Appl. Crystallogr.* **2011**, *44*, 1272-1276.
10. Crosby, G. A.; Demas, J. N., Measurement of photoluminescence quantum yields. *Review. J. Phys. Chem*. **1971**, *75*, 991.
11. Melhuish, W. H., Quantum Efficiences Of Fluorescence Of Organic Substances: Effect Of Solvent And Concentration Of The Fluorescent Solute 1. *J. Phys. Chem*. **1961**, *65*, 229.
12. Greenham, N.; Samuel, I.; Hayes, G.; Phillips, R.; Kessener, Y.; Moratti, S.; Holmes, A.; Friend, R., Measurement of absolute photoluminescence quantum efficiencies in conjugated polymers. *Chem. phys. lett.* **1995,** *241*, 89-96.
13. *CrystalClear-SM Expert v. 2.1*, Rigaku Americas, The Woodlands, Texas, USA, **2015**.
14. *CrysAlisPro* v1.171.38.46. Rigaku Oxford Diffraction, Rigaku Corporation, Oxford, U.K. **2015**.
15. G. Sheldrick; *Acta Crystallogr., Sect. C: Cryst. Struct. Commun.*, **2015**, *71*, 3-8.
16. Dolomanov, O. V.; Bourhis, L. J.; Gildea, R. J.; Howard, J. A. K.; Puschmann, H. *J. Appl. Crystallogr*. **2009**, *42*, 339-341.
17. Lin, L.; Fan, J.; Cai, L.; Wang, C. K., Excited state dynamics of new-type thermally activated delayed fluorescence emitters: theoretical view of light-emitting mechanism. *Mol. Phys*. **2018**, *116*, 19.
18. Hall, D.; Suresh, S. M.; dos Santos, P. L.; Duda, E.; Bagnich, S.; Pershin, A.; Rajamalli, P.; Cordes, D. B.; Slawin, A. M.; Beljonne, D., Improving Processability and Efficiency of Resonant TADF Emitters: A Design Strategy. *Adv. Opt. Mater.* **2020,** *8*, 1901627.